Numerical Modeling of the Sedimentation Process using Coupled Discrete Element Method and Computational Fluid Dynamics

F. Chen, M. Fredlund, SoilVision Systems Ltd.
P.S. Wells, Suncor

ABSTRACT

The mechanism of sedimentation and large-strain consolidation is well-known to occur in oil-sand tailings. The transition point between the processes remains ambiguous and subjects to continued research. Sedimentation has been generally considered to follow Kynch's theory however there are additional questions as to how closely the sedimentation follows theory. Recent studies undertaken by SoilVision Systems Ltd. and a client have endeavored to model sedimentation theory at a basic particulate level making use of combined Discrete Element Method (DEM) and Computational Fluid Dynamics (CFD).

The purpose of this study is trying to match simulation results to both theoretical and experimental results. Therefore two types of models are currently used: the model using pure spherical particles (sphere model) and a model using cylindrical clumps (clump model). The sphere model will be used to verify simulation results with Kynch's theory and the clump model will be used to simulate the sedimentation process of oil-sand tailings at a laboratory scale. The simulation procedures and the final results show that coupled DEM-CFD method can agree well with theoretical results and can also provide prediction for experimental results via calibration.

1 OVERVIEW OF THE THEORETICAL BACKGROUND

The mechanism of sedimentation and large-strain consolidation is well-known to occur in oil-sand tailings. The transition point between the sedimentation to consolidation processes remains ambiguous and thus subject to continued research. In this study, the Mature Fine Tailings (MFT) sedimentation process is investigated using coupled Discrete Element Method and Computational Fluid Dynamics (DEM-CFD) theory which treats the solid phase soil particles as discrete material while the fluid phase as a continuum. The fluid phase is modeled through an Eulerian model and the particle phase is modeled through a Lagrangian model by tracing the trajectory of each individual solid particle. This coupled simulation method is currently widely accepted and applied in both academic and industrial fields in the modeling process such as fluidized beds, hydro-dynamic transport of granular materials and many other fluid-particle two-phase flow systems. Theoretical details of the DEM-CFD coupled model can refer to (Tsuji et al. 1993) and (Chen et al. 2011) and will be applied in this sedimentation simulation study.

2 THE COUPLED DEM-CFD METHOD

In coupled DEM-CFD method, the fluid phase is treated on a macroscopic scale using a continuum approach with the finite volume method (FVM). The particle motion is described using the standard discrete element approach (DEM) proposed by (Cundall and Strack 1979). The different treatments of the two phases are described below.

2.1 Fluid phase governing equations

The governing equation for the fluid phase is the averaged Navier-Stokes equation (Anderson and Jackson 1967). The pressure and the velocity values of the fluid within each fluid cell are locally averaged.

The continuity equation is given below:

$$\frac{\partial n}{\partial t} + \nabla(nU) = 0 \quad (1)$$

The momentum equation is given below:

$$\frac{\partial nU}{\partial t} + \nabla(nUU) - \nabla\cdot(\mu\nabla U) = -\frac{n}{\rho_f}\nabla p + \frac{f_P}{\rho_f} \quad (2)$$

where n=porosity (void fraction); U=fluid velocity; t=time, p=fluid pressure, μ=fluid viscosity; ρ_f=fluid density; f_P= interaction force on the fluid per unit volume from the particle defined in Eq. (7).

2.2 Particle phase governing equations

In the current study, the following forces are considered for a single particle: gravity, buoyancy, contact forces from adjacent particles and drag force from the fluid flow. The equation of motion using Newton's 2nd law for each individual particle settling in fluid can be expressed as:

$$\frac{dv}{dt} = \left(f_{G,i} + f_{B,i} + f_{D,i} + f_{C,i} \right) / m \quad (3)$$

where dv/dt= particle i acceleration; $f_{G,i}$=gravitational force; $f_{B,i}$=buoyancy force; $f_{D,i}$=drag force acting on single particle i from the fluid; $f_{C,i}$=composite inter-particle force from adjacent particles and m=mass of a particle.

2.3 Inter-particle forces

The inter-particle force $f_{C,i}$ is the generalized adjacent particle forces acting on particle i, which includes both electrical charges force (Coulomb force) and contact forces from the other particles:

$$f_{C,i} = f_{Coulomb} + f_{contact} \quad (4)$$

2.3.1 Coulomb charges force

The electrical charges force $f_{Coulomb}$ is calculated via the general form of the Coulomb force expression given by Eq. (5):

$$f_{Coulomb} = k_e \frac{q_i q_j}{r^2} \quad \text{for } r < r_c \quad (5)$$

where k_e=8.99x10^{9}N.m^2.C^{-2}; q_i and q_j are the electric charges on the 2 particles; r_c is the cutoff distance, when the distance between particle i and j is greater than r_c, the charges force is 0.

2.3.2 Contact forces

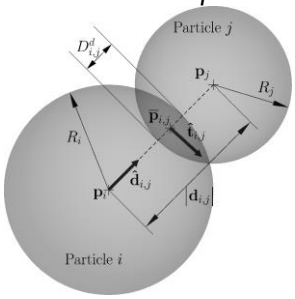

Figure 1. Simple inter-particle contact model (Weatherley 2009)

When two particles are in contact, the contacting forces between particle i and j $f_{Contact}$ is calculated through the mass-spring model with Hooke's law which assumes a simple linear force-displacement contact relationship as shown in Figure 1:

$$f_{contact} = kD_{i,j}^{d} \tag{6}$$

where $D_{i,j}^{d}$ is the overlap between the two particles as shown in Figure 1, k is the general contact stiffness between the two particles.

2.4 Fluid-particle interaction

The fluid-particle interactions are calculated through Newton's 3rd law of motion, i.e., the forces acting on the particles in a single fluid cell are equal to the forces acting to the fluid cell from the particles. The detailed relationship is presented by (Chen et al. 2011).

2.4.1 Interaction drag term on a single fluid cell

There have been several empirical drag correlation equations used in the two phase flow analysis, e.g. (Garg et al. 2012) and (Tsuji et al. 1993) to compute the interaction term f_P in the averaged Navier-Stokes equation in Eq. (2) most in the form similar to:

$$f_P = \frac{\beta}{\rho_f}\left(\bar{U}_P - U\right) \tag{7}$$

where $\bar{U}_P$ is the average particle velocity within a fluid cell, U is the fluid velocity within the cell (finite volume) and β is the empirical phase drag coefficient given by Ergun's (Ergun 1952) and Wen and Yu's (Wen and Yu 1966) empirical drag relationship in Eq. (9):

$$\beta = \begin{cases} \dfrac{\mu(1-n)}{d^2 n}\left[150(1-n)+1.75Re\right], & \text{for n<0.8} \\ \dfrac{3}{4}C_D\dfrac{\mu(1-n)}{d^2}n^{-2.7}Re, & \text{for n} \geq 0.8 \end{cases} \tag{8}$$

where the Reynolds number Re is defined as:

$$Re = \frac{\left|\bar{U}_P - U\right|\rho_f n d}{\mu} \tag{9}$$

and the drag coefficient C_D is:

$$C_D = \begin{cases} 24\left(1+0.15Re^{0.687}\right)/Re & \text{if } Re \leq 1000 \\ 0.43 & \text{if } Re > 1000 \end{cases} \tag{10}$$

2.4.2 Interaction drag force on a single particle

The drag force on particle from the fluid phase comes from two sources: (1) the pressure gradient within the fluid cell; (2) inter-phase drag due to the velocity difference between the particle and fluid. Therefore the drag force on a single particle $f_{D,i}$ is the sum of the two sources:

$$f_{D,i} = \frac{\beta}{1-n}\left(U - \bar{U}_P\right)V_{P,i} + \nabla p V_{P,i} \tag{11}$$

where $V_{P,i}$ is the single particle volume, there are two terms on the left hand side of Eq. (11), the first term is the phase drag and the other is the pressure force due to pressure gradient in the flow field.

2.5 Initial and boundary conditions for the solid and fluid phase

The purpose of this study is trying to match of our simulation results to both theoretical and experimental results. Therefore two types of models are currently used: the model using pure spherical particles (sphere model) to verify our simulation results with Kynch's theory and a model using cylindrical clumps (clump model) to calibrate our simulation to experimental results. The

sedimentation model is composed of solid and fluid two phases, therefore the structure of individual clumps, the overall packing arrangement for particle phase as well as the fluid domain geometry and boundary conditions for the fluid phase need to be specified separately. The methodologies adopted for each are shown in the following sections.

2.5.1 Random packing of spheres within the cylindrical tube

In order to verify our model to the theoretical Kynch's theory, a spherical packing of particles is generated within the cylindrical tube using the radial expansion method (Al-Raoush and Alshibli 2006). A sample packing of spheres is as shown in Figure 2a, the particles are in close distances so that the number of collisions between particles can be maintained during the simulation procedure.

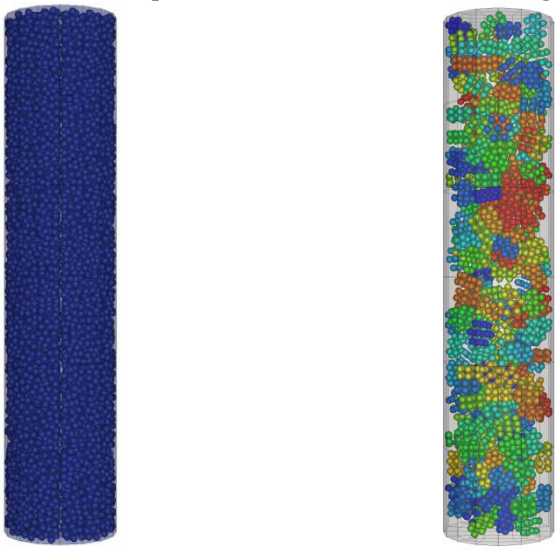

(a) (b)

Figure 2 Packing of spherical particles and clumps in the cylindrical tube

2.5.2 Construction of kaolinite and illite elements

The rigid clump concept is used to construct the kaolinite and illite elements. The kaolinite and illinite particles used in this study are simplified as shown in Figure 3. The diameter over height ratios of the clumps are kept at 2:1. For the illite clumps, one layer is assigned positive charge and the other layer is assigned negative charge; for the kaolinite clumps, the center particles are assigned the positive charges and the surrounding particles are assigned the negative charges.

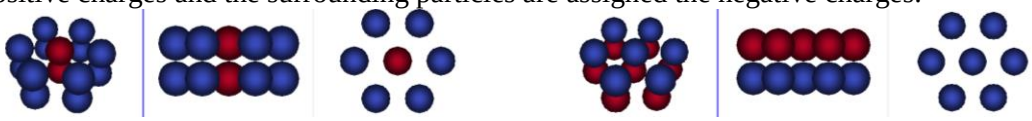

(a) kaolinite clump (b) illite clump

Figure 3 Construction of kaolinite and illite clumps from spheres

2.5.3 Random packing of clumps within the cylindrical tube

In order to calibrate our simulation results to experimental results, the random packing of kaolinite/illite clumps need to be generated as well. Packing for clumps is more difficult than spheres (Jia and Williams 2001). The packing algorithm adopted in the current study used a box-constrained algorithm by minimizing the distance between two adjacent spheres to a fixed tolerance (Martínez and Martínez 2003) and (Martínez et al. 2009). The result of a random 3D packing is shown in Figure 2b. A total number of 200 clumps are generated in Figure 2b with each clump colored by its unique ID number.

2.6 Initial and boundary conditions for the fluid phase

The fluid domain for the cylindrical tube is divided into a finite volume mesh as show in Figure 4. The ratio of mesh cell size compared to the diameter of the individual sphere is around 50 (by

packing volume) in order to obtain a meaningful porosity for each fluid cell. The boundary conditions of the fluid column are as shown in Table 1. According to the theoretical assumption of the coupled DEM-CFD model, each particle occupies its volume within the finite volume mesh. The total particle volume $V_{particle}$, the fluid volume V_{fluid} and the mesh volume V_{mesh} is related by the following equation:

$$V_{mesh} = V_{particle} + V_{fluid} \tag{12}$$

The porosity n is defined by:

$$n = 1 - \frac{V_{particle}}{V_{mesh}} \tag{13}$$

Table 1 Boundary conditions for the fluid domain

	Velocity (U)		Pressure (p)	
	Type	Value	Type	Value
Top	zeroGradient		fixedValue	0
Bottom	fixedValue	$U_x=U_y=U_z=0$	zeroGradient	
Cylinder Wall	fixedValue	$U_x=U_y=U_z=0$	zeroGradient	

2.7 Full (original) size and reduced size model

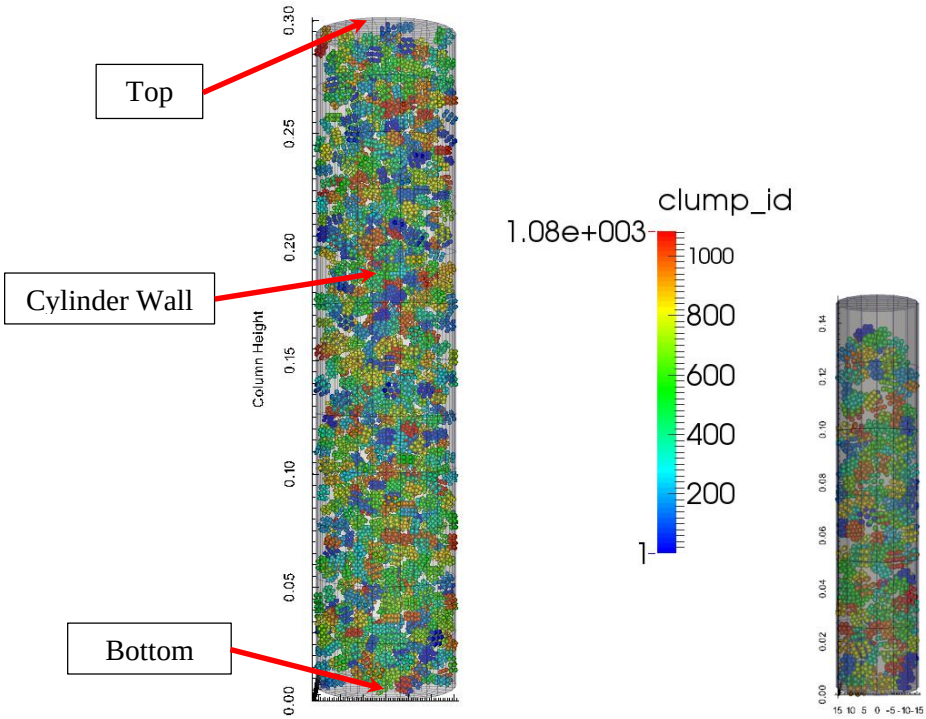

(a) Full size model (b) Reduced size model

Figure 4 Full size and reduced size model with packing of clumps (clumps colored by ID number)

A full size model was first constructed according to the size of the cylindrical tube used in the prototype experiments provided by the client as shown in Figure 4a. The full size cylinder model is 0.0325m in radius and 0.3m in height. The percent solids content used in the simulation are as shown in Table 3. In order to pack the full size model with the clumps defined in Figure 3 to meet the solids content, e.g. 15%, the packing procedure generated a total of 1084 clumps (which equals to a total of 15176 spheres). Due to the limitation of computational resources, a sedimentation model using this number of particles typically takes 48 to 60 hours to complete.

In order to save computation time and make it easier to enhance the parametric effects during the analysis, a reduced size model is currently used for the rest of the analyses in the report. The diameter and the height of the reduced size model are both reduced to 1/2 of the original cylindrical tube as shown in Table 2. The reduced size model can limit the simulation time to 6-10 hours and was proved to be able to illustrate the characteristics of the sedimentation similar to the full size model. Therefore the reduced half size model is used in the current study as shown in Figure 4b. The basic physical and geometry parameters used in the model are summarized in Table 2.

Table 2 Basic physical parameters used in the reduced size model

	Parameters	Value	Unit
DEM	Particle radius	0.001	m
	Particle density	2600	kg/m^3
	Contact stiffness	5.0E+06	N/m
	Restitution coefficient	0.3	
CFD	Cylinder column radius	0.01625	m
	Cylinder column height	0.15	m
	Fluid cell size dz	0.0125	m
	Fluid cell size dx	0.0040625	m
	Fluid cell size dy	0.0040625	m
	Fluid viscosity	8.94E-04	Pa.s
	Fluid density	1000	kg/ m^3

2.8 Scaling relationship between model and prototype particle sizes

The typical sizes of kaolinite/illite particles in the experiments are at 1μm level. In order to accommodate the large computational requirements, a factor of 1000 is used in the scaling relationship between model and prototype particle sizes: e.g. a 1.0mm model radius particle is used to simulate a prototype particle of radius 1.0μm. The scaling factor based on terminal velocity from Stokes equation (Batchelor 2000) is derived from Eq. (14):

$$u_\infty = \frac{1}{18}\frac{\left(\rho_p - \rho_f\right)d^2 g}{\mu} \tag{14}$$

where u_∞ is the terminal velocity of a single particle, ρ_p is the particle density, ρ_f is the fluid density, g is the gravitational acceleration, d is the diameter of the particle and μ is the fluid viscosity. When a solid particle falls through a fluid column from top to bottom due to gravity, the particle travels the same distance for both model and the prototype. In the current sedimentation model, it is assumed that all particles have reached their equilibrium state in the fluid and the sedimentation time is mainly controlled by the terminal velocity of the particle. Based on Eq. (14), the terminal velocity of model and prototype can be determined as:

$$\frac{u_{\infty,m}}{u_{\infty,p}} = \frac{d_m^2}{d_p^2} \tag{15}$$

where d_m is the model particle diameter and d_p is the prototype particle diameter. When using a scaling factor of 1000 (d_m/d_p=1000), the ratio of the terminal velocity between model and prototype is 1.0E+6, the time needed for the model (T_m) and prototype (T_p) to complete their respective sedimentation process is then the inverse of the diameter ratio:

$$\frac{T_p}{T_m} = \left(\frac{d_m}{d_p}\right)^2 = 1.0 \times 10^6 \quad (16)$$

For a DEM-CFD model simulation time of 1.0s, the scaled prototype time will be 1.0E+6sec which corresponds to 46 days. However note that due to complicated particle interactions in a hindered settling environment where the actual sedimentation time is determined by many other factors, the scaling factor has to be determined in accordance with the actual sedimentation curve which will be detailed in section 4.2. In the following sections, a time scaling factor of 9.49E+05 (close to 1.0E+6) determined from section 4.2.3 is used so that a simulation time of 64.0s can represent real time sedimentation of 703 days. The determination of 64.0s simulation time is according to the observation from the DEM-CFD model results when the entire sedimentation process is roughly complete.

3 THE SIMULATION PROCEDURE

After the initial packing of the particles is generated with the fluid column, the simulation is then started and the results of the sedimentation including the physical properties of both particle phase and fluid phase are recorded every certain number of time steps.

3.1 The sedimentation procedure of the sphere model

The sphere model is used to compare the simulation results with the Kynch's theory. Serialized snapshots for the sphere model showing the entire sedimentation process up to a real time 77d is summarized in Figure 5. The flow field is colored by the fluid velocity magnitude of each cell. It can also be seen from Figure 5 that the flow fields (fluid velocity) for all snapshots are close to zero with little to no variation, this is consistent with Concha's conclusion (Concha 2013) for sedimentation at small Reynolds number where convective acceleration may be neglected in the Navier-Stokes equation.

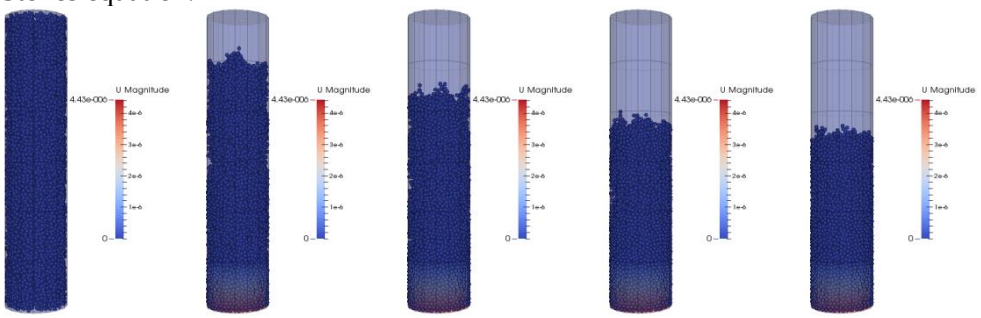

Figure 5 Selected screenshots showing the sedimentation process of sphere model at different times (t=0d to t=77d, flow field colored by the fluid velocity magnitude of each cell)

3.2 The sedimentation procedure of clump model

The clump model is used to compare the simulation results with the experimental results. Serialized snapshots for the clump model showing the entire sedimentation process for the client RP-07A (refer to Table 3) sample up to a real time 77d is summarized in Figure 6. The flow field is colored by the fluid velocity magnitude of each cell similar to section 3.1. It can also be interpreted from Figure 6 that the flow fields (fluid velocity) for all snapshots are close to zero with little to no variation which is similar to the sphere model case. The observed flow velocity field is in a reasonable uniform state with only some small variation at the bottom of the column (Concha 2013).

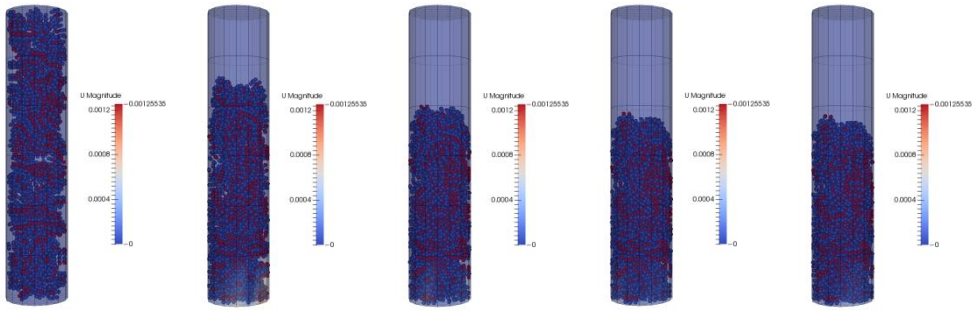

Figure 6 Screenshots showing the sedimentation process of clump model at different times (t=0d to t=77d, flow field colored by the fluid velocity magnitude of each cell)

4 DISCUSSION OF RESULTS

The simulation results are compared to both theoretical and experimental results shown below.

4.1 Comparison of the sedimentation curve to Kynch's theory using spherical particles

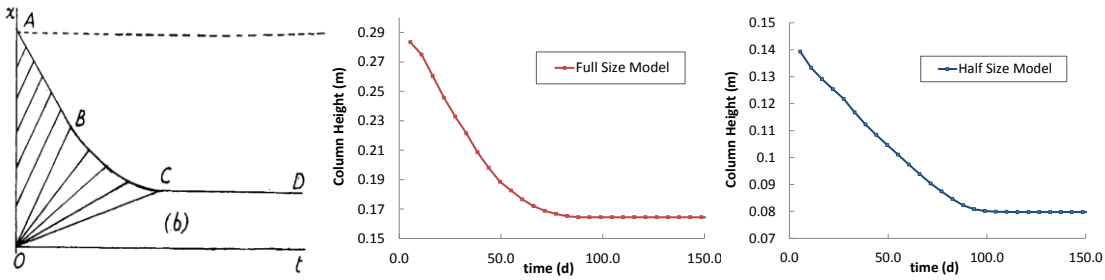

(a) Kynch's theory curve (b) Full size model curve (c) Reduced size (half) model curve

Figure 7 Comparison of theoretical results with DEM-CFD simulation results

The spherical particles model is setup with the purpose to compare with the shape of sedimentation curve given by Kynch's theory (Kynch 1952) in order to verify the conceptual correctness of the coupled DEM-CFD methodology. The sedimentation curves of the DEM-CFD simulated results using both the full size model and reduced sized model are as shown in Figure 7. The shapes of the simulated curves agree well with the curve from Kynch's theory. Due to the difficulty of finding a numerical example, the comparison with Kynch's theory is done at the conceptual level at this moment. More detailed comparison can be a topic of future research.

4.2 Calibration of the sedimentation curve to experimental results

From the simulation results, given sufficient time for the entire sedimentation process to complete, a typical sedimentation curve of a particle assembly with the presence of charges force can be roughly divided into 3 linear stages as shown in Figure 8: the first sedimentation stage has the largest slope (slope 1), the second transition stage has an intermediate slope (slope 2) while the consolidation stage has the smallest slope (slope 3) when the clumps are being consolidated and the stresses are developing from the bottom of the particle assembly.

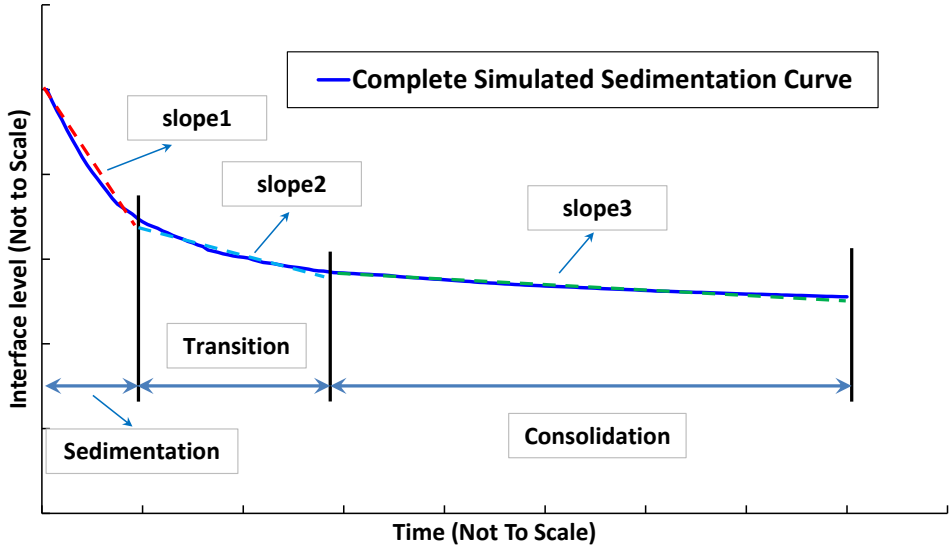

Figure 8 A complete sedimentation curve from coupled DEM-CFD analysis using clump

4.2.1 Overview of the experimental results

The four settling graph and picture of settling column for BEU middlings sedimentation experiments obtained from the client (RP-04A, RP-05A, RP-07A, RP-15A) are as shown in Figure 9, the four curves are plotted together for comparison purpose in Figure 10. The physical parameters for all samples are listed in Table 3. The curves shown in Figure 10 all display two-stage sedimentation behavior: from 0 day to around 10 days is the sedimentation stage where the MFT mixture settles and the fall slope of the interfacial level is steep, from 10 days to 130 days, all curves enter a linear portion. Compared to the entire simulation curve shown in Figure 8, none of the four experimental curves has reached the consolidation stage where the change of the interface level (slope 3 in the sedimentation curve in Figure 8) is much smaller than the first two stages. It is also noted that from Table 3 the percent solids content does not appear to determine or affect the shape of the sedimentation curve.

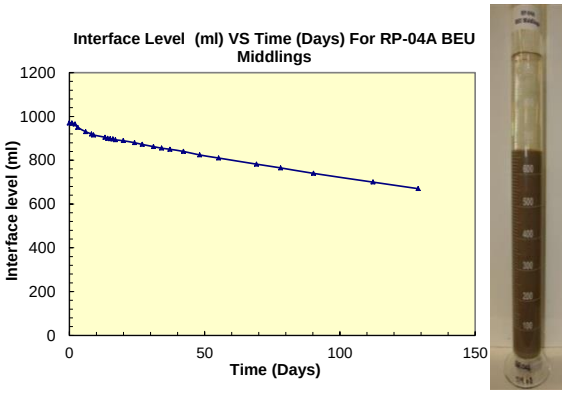

BEU RP-04A

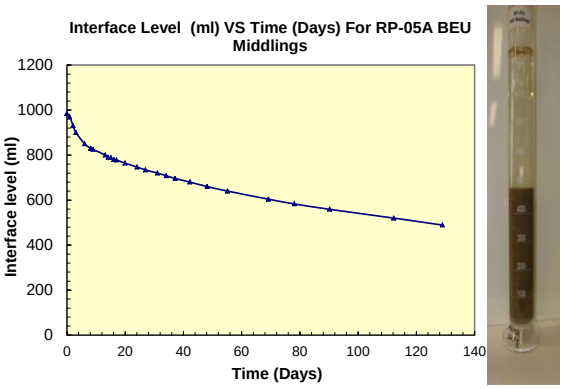

BEU RP-05A

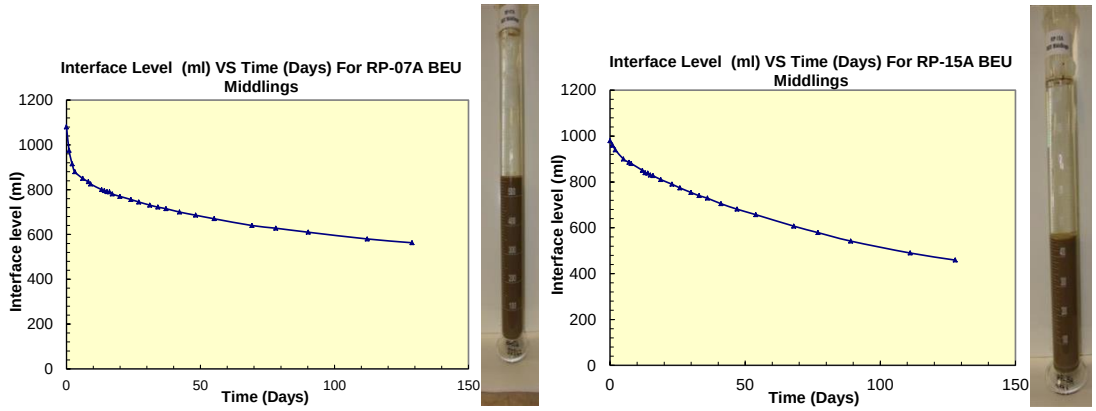

BEU RP-07A BEU RP-15A

Figure 9 Experimental sedimentation curves and settling column pictures of the four client BEU middling samples

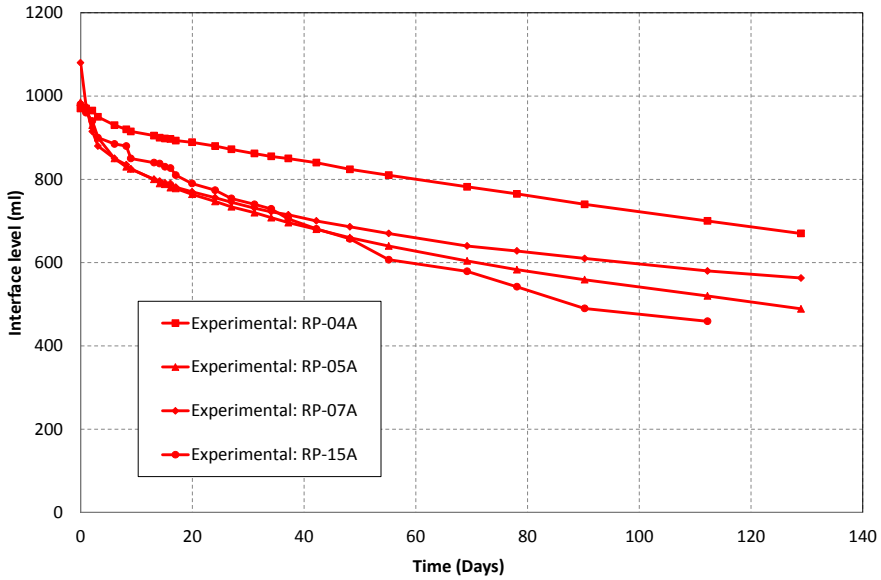

Figure 10 Summary of all 4 experimental sedimentation curves

Table 3 Major physical parameters for the 4 experimental samples*

Sample	Density (g/ml)	Volume (ml)	Temperature (°C)	% solids
RP-04A	1.04	975	21.1	7.37
RP-05A	1.03	987	21.5	6.35
RP-07A	1.09	1080	21.7	15.42
RP-15A	1.03	980	22.1	6.97

*The diameter of the settling column is 65mm.

4.2.2 The calibration process

It is relatively difficult to tell the cause of the difference of the four experimental curves shown in Figure 10 and it is also difficult to quantify the exact physical parameters which exist in the experimental samples. However, it is helpful to calibrate the simulation curves to the shape of the experimental curves so that a general pattern or trend of the entire curve can be predicted using current known simulation parameters.

Table 4 Basic simulation parameters used in the calibration process

Parameters	Value	Unit
Volume (half size model)	125	ml
Density (15% solids content)	1.06	g/ml

Fluid viscosity (water @25ºC)	8.94E-04	Pa.s
Split percentage between illite and kaolinite	50	%
Particle radius	0.001	m
Boundary friction coefficient	0.5	

The model parameters used to calibrate the model curve to the experimental curves are as listed in Table 4. The reduced DEM-CFD models are controlled so that the density, volume and temperature values are very close to the 4 client BEU middling experimental configurations. In addition to the time scaling factor of 9.49E+05 mentioned in section 2.8, from various sensitivity analysis of different simulation parameters, it is found that varying the electrical charges on the model can change the intermediate slope (slope 2) of the simulation curve, the amounts of the electrical charges used for each of the four simulation curves are adjusted using the values shown in Table 5 so that the linear portion of the curves (slope 2 in Figure 8) can match the corresponding experimental curves, the sensitivity analysis details will be discussed in a separate publication.

Table 5 Charges amount used for calibration of the 4 simulation curves

Sample	Charges (Unit: Coulomb)
RP-04A	3.930E-10
RP-05A	3.144E-10
RP-07A	3.537E-10
RP-15A	2.751E-10

By visually comparing model and prototype sedimentation curves, the simulation curves are all scaled so that the first two stages of the simulation curves can roughly match the experimental curves. The same procedure is repeated for all 4 experimental curves. Due to a limitation of the code used, all simulation curves use 15% solids content for the calibration, the results of the calibration are shown in section 4.2.3.

4.2.3 Comparison of calibrated simulation curves to experimental curves

All four comparisons of calibrated simulation curves versus experimental curves are as shown in Figure 11. The two groups of curves agree quite close to each other with the exception of some minor differences at very early stages.

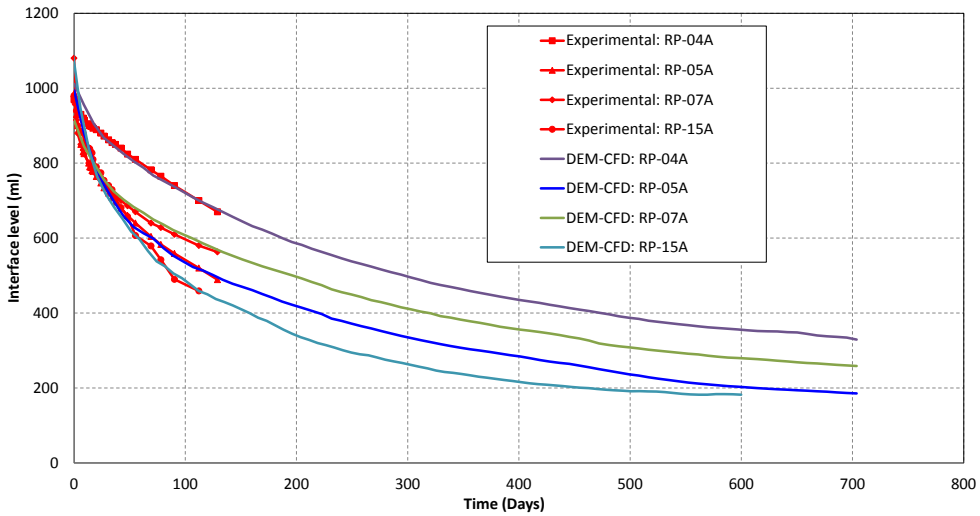

Figure 11 Summary of comparison between calibrated simulation curves and experimental results

4.3 Prediction of the consolidation stage of experimental curves from calibration

The calibrated simulation curves in Figure 11 are able to show all three stages of the MFT sedimentation process. While it is difficult to quantify the exact physical parameters inside a real

experimental MFT sample, it is still instructive to use calibrated curves to "extrapolate" the trend of the experimental results and predict the experimental sedimentation behavior. From Figure 11, the slopes of all four simulation curves at the end all tend to zero (flat) which indicates that the consolidation is close to complete. Based on this calibration/scaling, a rough estimate of the time necessary for the experimental sample to complete the consolidation is around 703 days, i.e., it will take the laboratory MFT samples about 2 years to transit from settlement to consolidation and then complete the consolidation process.

5 CONCLUSIONS AND FUTURE RECOMMENDATIONS

The DEM-CFD model deployed in this study is capable of simulating the laboratory scale sedimentation process by using proper packing algorithm for the solid phase and applying reasonable boundary conditions for the fluid phase similar to the experimental conditions. The simulated sedimentation curves can match theoretical results and calibrate to experimental curves. In summary, the current work has made the following contributions to the study of the MFT sedimentation process:

1) The current DEM-CFD model can conceptually compare the simulation curve to Kynch's theory.
2) The coupled DEM-CFD approach is capable of simulating the MFT sedimentation process and can provide comparable sedimentation curves with the laboratory scale results through scaling law.
3) The calibrated simulation curves give a rough estimation of 2 years (703 days) for all 4 experimental curves to complete the consolidation.

Due to the limitation of available computational resources, the particle (sphere) used in the current simulation is 1.0mm radius which corresponds to a prototype particle radius of 1.0μm, Results even closer to the experimental observations could be obtained by utilizing more computational resources with larger scale simulation of more number of particles.

6 REFERENCES

Anderson, T. B., and Jackson, R. (1967). "Fluid Mechanical Description of Fluidized Beds. Equations of Motion." *Industrial & Engineering Chemistry Fundamentals*, 6(4), 527–539.

Batchelor, G. K. (2000). *An Introduction to Fluid Dynamics*. Cambridge University Press.

Chen, F., Drumm, E. C., and Guiochon, G. (2011). "Coupled discrete element and finite volume solution of two classical soil mechanics problems." *Computers and Geotechnics*, 38(5), 638–647.

Concha, F. (2013). *Solid-Liquid Separation in the Mining Industry*. Springer International Publishing.

Cundall, P. A., and Strack, O. D. L. (1979). "A discrete numerical model for granular assemblies." *Géotechnique*, 29(1), 47–65.

Ergun, S. (1952). "Fluid flow through packed columns." *Chemical engineering progress*, 48, 89–94.

Garg, R., Galvin, J., Li, T., and Pannala, S. (2012). "Open-source MFIX-DEM software for gas–solids flows: Part I—Verification studies." *Powder Technology*, 220, 122–137.

Jia, X., and Williams, R. A. (2001). "A packing algorithm for particles of arbitrary shapes." *Powder Technology*, 120(3), 175–186.

Kynch, G. J. (1952). "A theory of sedimentation." *Transactions of the Faraday Society*, 48(0), 166–176.

Martínez, J. M., and Martínez, L. (2003). "Packing optimization for automated generation of complex system's initial configurations for molecular dynamics and docking." *Journal of Computational Chemistry*, 24(7), 819–825.

Martínez, L., Andrade, R., Birgin, E. G., and Martínez, J. M. (2009). "PACKMOL: a package for building initial configurations for molecular dynamics simulations." *Journal of Computational Chemistry*, 30(13), 2157–2164.

Al-Raoush, R., and Alshibli, K. A. (2006). "Distribution of local void ratio in porous media systems from 3D X-ray microtomography images." *Physica A: Statistical Mechanics and its Applications*, 361(2), 441–456.

Tsuji, Y., Kawaguchi, T., and Tanaka, T. (1993). "Discrete particle simulation of two-dimensional fluidized bed." *Powder Technology*, 77(1), 79–87.

Weatherley, D. (2009). *ESyS-Particle v2.0 user's guide*. The University of Queensland, Earth Systems Science Computational Centre (ESSCC).

Wen, C. Y., and Yu, Y. H. (1966). "A generalized method for predicting the minimum fluidization velocity." *AIChE Journal*, 12(3), 610–612.